

Robot peels banana with goal-conditioned dual-action deep imitation learning

Heecheol Kim^{1,2}, Yoshiyuki Ohmura¹, Yasuo Kuniyoshi¹

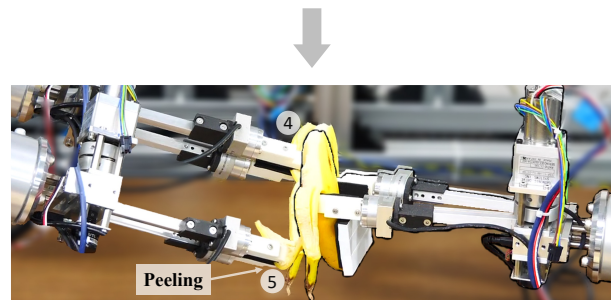
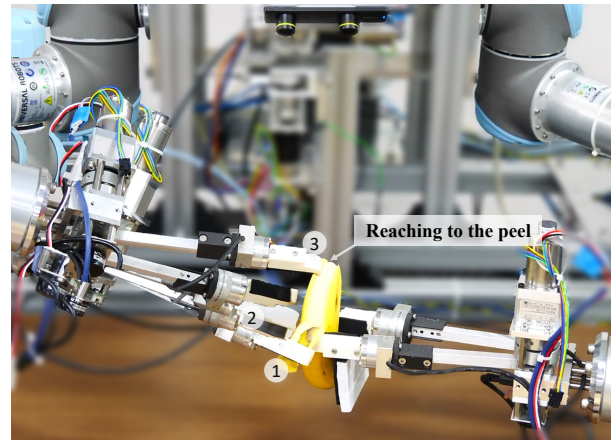
Abstract—A long-horizon dexterous robot manipulation task of deformable objects, such as banana peeling, is problematic because of difficulties in object modeling and a lack of knowledge about stable and dexterous manipulation skills. This paper presents a goal-conditioned dual-action deep imitation learning (DIL) which can learn dexterous manipulation skills using human demonstration data. Previous DIL methods map the current sensory input and reactive action, which easily fails because of compounding errors in imitation learning caused by recurrent computation of actions. The proposed method predicts reactive action when the precise manipulation of the target object is required (local action) and generates the entire trajectory when the precise manipulation is not required. This dual-action formulation effectively prevents compounding error with the trajectory-based global action while respond to unexpected changes in the target object with the reactive local action. Furthermore, in this formulation, both global/local actions are conditioned by a goal state which is defined as the last step of each subtask, for robust policy prediction. The proposed method was tested in the real dual-arm robot and successfully accomplished the banana peeling task.

Index Terms—Imitation Learning, Deep Learning in Grasping and Manipulation, Dual Arm Manipulation, Force and Tactile Sensing, Telerobotics and Teleoperation

I. INTRODUCTION

DEEP imitation learning, which trains the robot’s behavior using human-generated demonstration data with deep neural networks, is promising because this can transfer the implicit human knowledge of dexterous manipulation into a robot system without a pre-defined manipulation rule of knowledge of objects [1]–[4].

This paper presents deep imitation learning to achieve dexterous robot manipulation tasks such as banana peeling (Fig. 1) with a general-purpose dual-arm robot manipulator. In this task, every banana’s shape, size, and skin pattern are different, making the banana model acquisition difficult. Also, the deformation of bananas during peeling makes this task even more difficult. Because the banana is deformable, soft, and easily breakable, the robot has to tear its peel while maintaining its body; it requires highly dexterous manipulation skills that consider physical interactions with the target object, which is difficult for rule-based robotics. The banana peeling is a long-horizon task that includes several reaching and peeling subtasks and requires stable manipulation policies



(a) A part of the automated banana peeling sequence that the robot reaches its end-effector to the banana peel (1 ~ 3) and peels it (4 ~ 5).



(b) Example bananas used in the evaluation.

Fig. 1. The proposed goal-conditioned dual-action imitation learning (GC-DA) can peel the real banana of various shapes (1b) with a general-purpose dual-arm robot.

for consecutive success on each subtask. Therefore, to our knowledge, no previous robotics research handled this task.

Previous deep learning-based object manipulation methods required annotated keypoints and used manually defined manipulation rules (e.g., [5]–[9]). However, these methods cannot be applied to complex manipulation tasks of which the robot has to actively adapt its manipulation skills along with the changes of object states. The banana peeling is one example of such a task. Therefore, a model-free deep imita-

¹ Laboratory for Intelligent Systems and Informatics, Graduate School of Information Science and Technology, The University of Tokyo, 7-3-1 Hongo, Bunkyo-ku, Tokyo, Japan (e-mail: {h-kim, ohmura, kuniyoshi}@isi.imi.i.u-tokyo.ac.jp, Fax: +81-3-5841-6314)

² Corresponding author

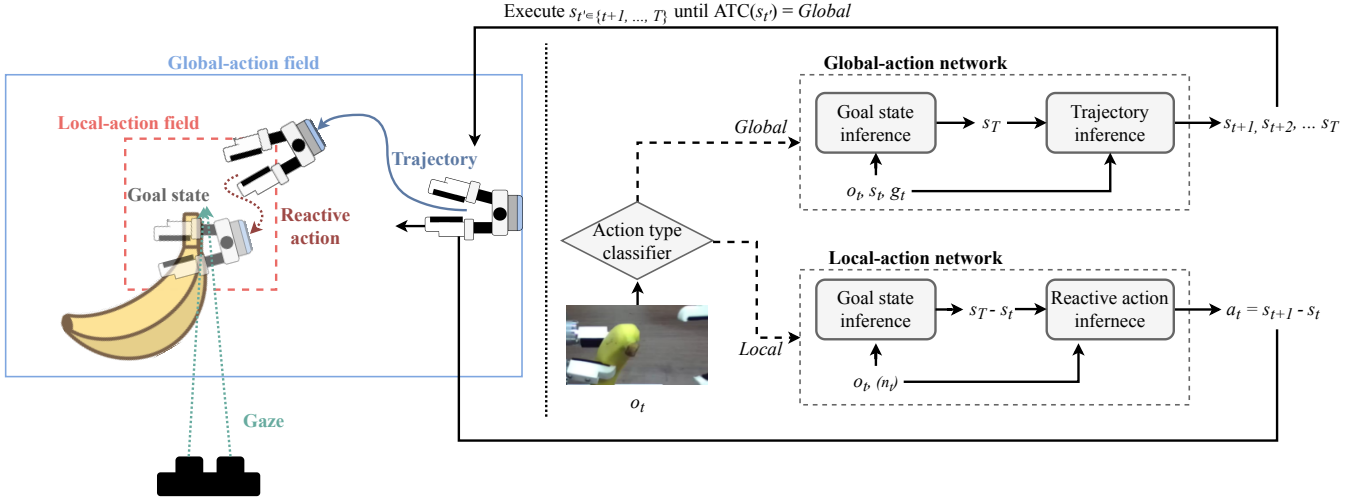


Fig. 2. Proposed *GC-DA* architecture. The action type classifier (ATC) determines if precise manipulation of the target object is required ; if not, the global-action network computes trajectory of the end-effector which is robust against compounding errors, if so, the local-action network computes reactive action that can dexterously manipulate the target object. o_t , n_t , s_t , g_t , a_t , and T refer to the foveated image, force/torque sensory values, robot kinematics states, gaze position, action, and last timestep in the sequence, respectively.

tion/reinforcement learning-based method (e.g., [1], [2], [10], [11]) is required, as they do not need any previously defined annotations or rule-based manipulation skills. However, simple visuomotor policy mapping requires too much demonstration data or exploration in tasks with long-horizon and high variation of target objects, such as banana peeling, which is infeasible in a real robot environment. These challenges make the banana peeling task interesting, providing a breakthrough to the limitations of the current robot manipulation research.

Our previous research proposed a visual attention-based deep imitation learning framework [12] that can focus on an important area of visual input by using a gaze signal of a human expert while demonstrating the task. Then, [3] proposed a dual-resolution dual-action system that separates local action in the vicinity of the gaze position and global action outside of the gazed area, which succeeded in dexterous manipulation tasks such as needle threading. However, the dual-resolution dual-action system was applied to tasks where the objects are located in two-dimensional space, which is relatively narrow than the banana peeling task and the state variation of needle is narrow because the needle is not deformable. Therefore, the previous dual-resolution dual-action system cannot provide sufficient precision and data efficiency for banana peeling task.

In the previous dual-action system, both global and local actions are reactive actions, which is the difference between next step state and current state: $a_t = s_{t+1} - s_t$, where a_t is the reactive action and s_t is the robot kinematic state. This reactive action can respond to unexpected immediate changes in the environment caused by incomplete environment model and error in policy predictions. However, because the reactive action changes the robot state recurrently, in the long-horizon tasks, the state eventually escapes from the training distribution by compounding error in action prediction. Besides, if the agent predicts the entire trajectory, the problems caused by

the compounding error occur less, but the trajectory-based manipulation cannot deal with immediate changes in the environment.

We hypothesize that in the manipulation task, the immediate changes in the environment usually occur while the end-effector is interacting with the target object. Therefore, if the end-effector is in the vicinity of the object, reactive action is required; if not, trajectory-based action can stably transport the robot to near the goal position.

Based on the hypothesis described above, we propose a method that uses reactive action for dexterous manipulation and trajectory-based action for robustness against compounding error (Fig. 2). This architecture separates local action from the sequence of the robot behavior, and the local action is defined as the reactive action output from the visually attended feature input images using robot gaze (foveated images). The global action is a trajectory $s_{t+1}, s_{t+2}, \dots, s_T$, where T indicates the last step in the sequence, computed from the foveated image, current robot kinematic state, and gaze position. A simple CNN-based classifier can switch the action between global and local action, based on a criterion that considers if precise control of the target object is required.

This research also improves manipulation performance by predicting goal state, which is defined as the robot's kinematic state at the last timestep of each subtask, and goal-conditioned action inference. Previous deep imitation learning methods predict reactive action from input states of the current timestep [1], [2], [12]. However, action should also be conditioned by goal state because the action can be considered a part of the route from the current state to the goal state; therefore, the action has to be changed if the goal state is changed. The neural network only statistically maps the action from the current sensory input state without goal conditioning, which is fragile to distractions in the input state. Therefore, the

proposed model first predicts the goal state, which is defined as the last state in the sequence, then the action is predicted using the goal state and the current sensory input state to achieve robust policy prediction.

The proposed goal-conditioned dual-action (*GC-DA*) imitation learning model was tested with the banana peeling task in the real dual-arm robot manipulator (UR5).

II. RELATED WORK

A. Trajectory-based methods for robot manipulation

Trajectory generation methods have been studied widely in robotics (e.g., [13], [14]). For example, [15] studied searching trajectory in reinforcement learning using factorized-action variational autoencoder [16]. Notably, in path planning methods in which a robot plans its path to the goal while avoiding obstacles, global path planning and local path planning are present. Global path planning plans the entire path using global information [17]–[20]. On the other hand, the local path planning computes real-time reactive action based on local information and is robust to the unpredicted disturbance in the environment [21]–[24]. The hierarchical planners that combine global and local path planning achieved collision-free motion without delays caused by the local path planner [25]. This method support our system that combines trajectory-based global action and reactive local action. Nevertheless, the path planning-based methods cannot be directly applied to our target task because acquiring the deformable and high-variance object model from visual sensory input is difficult, and both path planning and reactive action with the target object is unknown.

B. Goal-based policy learning

Goal-based policy learning has been studied in many different aspects. [10], [26], [27] considered goal while policy searching during manipulation. [10] proposed hindsight experience replay (HER), which assumes the last state in an explored episode as a goal, even though the episode was not successful. This goal is used for a data-efficient training of a goal-conditioned policy. [26] applied HER to generative adversarial imitation learning (GAIL) [28], which uses generative adversarial training [29] for reward learning to leverage policy convergence speed. [27] acquired dense reward using goal proximity function trained from demonstration data. However, exploration-based methods cannot be applied to our task setup, which has to train dexterous robot policy only using a limited number of bananas as training data.

Researches did not rely on additional exploration except for demonstration are [30]–[36]. [30]–[33], [36] applied goal to help predict the policy. [30], [31] used user-provided goal scenes to select pre-defined manipulation behavior from an axiomatic scene graph of current visual input. These methods successfully manipulated objects in long-horizon tasks in cluttered scenes. [34], [35] selected high-level action using goal-based imitation, and low-level actions are pre-defined. [32], [33] inferred the primitive action from the goal. [32] trained a latent variable model using variational autoencoder [37] to control a robot manipulator to the given goal. [33]

proposed a neural network architecture conditioned on high-level commands on autonomous driving. In these methods, the goal is an externally provided signal to change the agent’s behavior. On the other hand, in our proposed method, the goal prediction and conditioning is applied to achieve stable and dexterous manipulation policy.

[2] leveraged manipulation accuracy by training the auxiliary prediction, which expects the gripper’s position when closed during picking. Furthermore, [36] predicts a state fixed timesteps apart as a goal then computes the goal-conditioned action. Therefore, these experimental results support our idea that the goal-conditioned neural network can provide better manipulation accuracy for manipulation. In our research, the explicit goal prediction and conditioning method for dual-action architecture is proposed and used for dexterous manipulation.

C. Automation in food processing

Researches on food processing automation using robots include food manufacturing in factories [38], [39], fruit harvesting [40]–[45], and cooking [46], [47]. Many of these studies relied on task-specific end-effector design [44], [45], [48], [49] or rule-based manipulation [40]–[42]. Therefore, these researches lacked the acquisition of dexterous manipulation skills; limited the target task to simple object manipulations such as pick-and-place. On the other hand, this research uses a general-purpose one-degree of freedom end-effector, which can also be applied to other various tasks [3], [4], [12], [50], to peel bananas by imitating human manipulation skills. To our knowledge, there has been no study that applied deep imitation learning in food processing.

III. METHOD

A. Robot framework

This research uses a dual-arm robot framework for imitation learning which was also used in our previous researches (e.g., [3], [12]). This framework consists of a dual-arm robot system with two UR5 (Universal Robots) manipulators and two controllers with identical kinematic parameters with the UR5 robot. Demonstration data is generated by controlling robots with the controllers. A ZED mini stereo camera (StereoLabs, [51]) is mounted on a robot system with a two-dimensional pan-tilt structure. In this research, the camera is fixed on a position that can observe bananas (pan: 0 rad, tilt: -0.9 rad). The human operator can see the stereo camera image with a head-mounted display (HMD) while operating the robot. Furthermore, an eye tracker (Tobii) is mounted on the HMD to measure the operator’s gaze position in real-time.

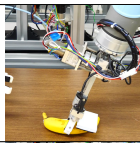
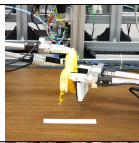
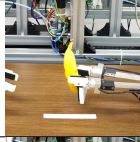
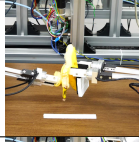
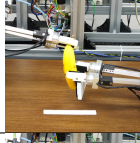
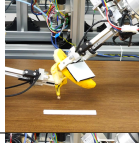
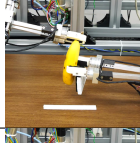
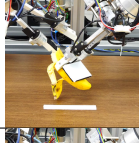
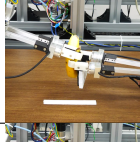
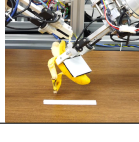

B. Task specification

The banana peeling task is long-horizon and can be segmented into several subtasks. The segmentation into each subtask is conducted under a criterion that whether each subtask’s goal state can represent its sequence (Table I):

- *GraspBanana*: The left hand grasps the banana on the table.

TABLE I

SUBTASK DETAILS AND ITS VISUAL EXAMPLE AT THE GOAL. ATC INDICATES IF AN ACTION TYPE CLASSIFIER (ATC) IS REQUIRED TO DETECT THE TRANSITION FROM GLOBAL TO LOCAL (OR LOCAL TO GLOBAL) ACTION. NSC REFERS IF THE NEXT SUBTASK CLASSIFIER (NSC) IS REQUIRED TO DETECT THE END OF THE SUBTASK SO THAT THE NEXT SUBTASK CAN BE EXECUTED. ALL SUBTASKS END WITH LOCAL ACTIONS THAT REQUIRE THE NSC. ASTERISK IS ONLY USED FOR CONSECUTIVE PEELING SETUPS.

Index	Subtask	Goal	Network type	ATC	NSC	Index	Subtask	Goal	Network type	ATC	NSC
1	<i>GraspBanana</i>		Global	✗	✗	7	<i>ReachRight</i>		Global → Local	✓	✓
2	<i>PickUp</i>		Global	✗	✗	8	<i>PeelRight</i>		Local → Global	✓	✗
3	<i>GraspTip</i>		Global → Local	✓	✗	9	<i>Reposition</i>		Global	✗	✗
4	<i>Push*</i>		Hand-crafted	✗	✗	10	<i>ReachLeft</i>		Global → Local	✓	✓
5	<i>PeelTip</i>		Local → Global	✓	✗	11	<i>PeelLeft</i>		Local → Global	✓	✗
6	<i>Rearrange</i>		Rearrange	✗	✗						

- *PickUp*: Lift up the grasped banana.
- *GraspTip*: The right hand reaches and grasps the banana tip.
- *PeelTip*: Peel the banana tip.
- *ReachRight*: The right hand moves close to contact the right peel.
- *PeelRight*: The right hand holds the peel and tears the peel.
- *Reposition*: Rotates the banana so that the right hand is reachable to the left peel.
- *ReachLeft*: The right hand moves close to contact the left peel.
- *PeelLeft*: The right hand holds the left peel and tears it.

For example, *GraspBanana*'s sequence can be explained by the left hand's goal kinematic state that grasped the banana. On the other hand, this sequence cannot be explained by *PickUp*'s goal kinematic state, which holds the banana. Therefore, *GraspBanana* and *PickUp* are separated.

Another possible strategy for banana peeling is to re-grasp the banana with the right hand and peel the left side with the left hand. However, the banana may become unstable after the re-grasping. Therefore, the banana is rotated rather than re-grasped.

Dataset	Number of demos	Total demo time (min)
<i>GraspBanana</i>	2050	89.9
<i>PickUp</i>	2073	63.2
<i>GraspTip</i>	2141	80.9
<i>PeelTip</i>	256	35.6
<i>ReachRight</i>	4458	211.6
<i>PeelRight</i>	264	27.4
<i>Reposition</i>	1779	41.3
<i>ReachLeft</i>	4009	237.6
<i>PeelLeft</i>	289	23.7
<i>Total</i>	17319	811.1

TABLE II
TRAINING SET STATISTICS.

During demonstrations, because the number of bananas is limited, non-destructive subtasks are repeated to maximize the number of demonstrations. *GraspBanana*, *PickUp*, *GraspTip*, *ReachRight*, *Reposition*, and *ReachLeft* do not tear or break the target banana; therefore, those subtasks are repeated 10 ~ 20 times per banana. On the other hand, *PeelTip*, *PeelRight*, and *PeelLeft* peel the bananas; therefore, these subtasks are non-reversible. Thus these subtasks are recorded only once per banana. All demonstrations were recorded at 5 Hz. Table II explains statistics of each subtask.

The banana peeling sequence is conducted in order of the above subtasks. On each subtask, the proposed dual-action which is composed of the trajectory-based global action and reactive local action is applied in the following manners:

- *GraspBanana, PickUp, Reposition*: These tasks do not require high precision manipulation. Therefore, for simplicity, these tasks are conducted only from trajectory-based global action.
- *GraspTip, ReachRight, ReachLeft*: These tasks require high-precision manipulation. Therefore, these tasks use the proposed dual-action architecture by approaching the target with global action and then accurately reaching the target with reactive local action.
- *PeelTip, PeelRight, PeelLeft*: Opposite to the reach subtasks, peel subtasks first controls the end-effector near the target banana, and their correlation gradually diminishes during peeling. Therefore, these subtasks first use local action, then execute global action.

C. Goal-conditioned dual-action

Figure 2 and Algorithm 1 illustrate the concept of goal-conditioned dual-action. The dual-action-based architecture separates the reactive local action, which is used when the precise control is required, from the trajectory-based global action, used when the path planning robust against the compounding error is required.

The boundary between local action and global action is decided by whether the robot requires the precise manipulation. This boundary decision is annotated by humans then trained with a binary classifier to autonomously switch between global and local action (see III-E for details). Notably, on high-precision reaching subtasks, simple criterion whether the end-effector is in the foveated image can decide the boundary (see Appendix A for details).

Both global and local actions are conditioned by the goal state, the robot kinematic state at the last timestep T of the sequence in each subtask. Simple end-to-end imitation learning $a_t = s_{t+1} - s_t = \pi(e_t)$, where π , e_t , s_t , and a_t refer to the policy, embedding of current input states, robot kinematic state, and current action, which maps s_t to a_t , is unstable to the distractions in s_t . On the other hand, the explicit inferred goal state s_T , where T refers the last timestep in the sequence, can provide stable policy because the action can use explicit information of the task goal. The trajectory-based global-action network first predicts the goal state: $s_T = \pi_{global}^{goal}(e_t)$, where s_T and π_{global}^{goal} refers to the inferred robot kinematic goal state and the goal predictor of the global-action network. Then, the trajectory $s_{t+1}, s_{t+2}, \dots, s_{T-1}$ is predicted using both e_t and s_T : $s_{t+1}, \dots, s_{T-1} = \pi_{global}^{policy}(e_t, s_T)$, where π_{global}^{policy} refers to the policy inference of the global-action network. For subtasks except for *GraspBanana, PickUp*, and *Reposition*, which are only composed of global action, the predicted trajectory is executed during $ATC(o_{t \in \{t+1, \dots, T\}}) = global$, where ATC indicates the action type classifier.

The reactive local-action network only inputs the foveated image o_t because the reactive local action can be computed efficiently from the relation between the target object and

Algorithm 1 Goal-conditioned dual-action deep imitation learning

Parameter: Action type classifier ATC , Global-action network π_{global} , Local-action network π_{local} , gaze predictor ρ

```

1:  $t \leftarrow 0$  {initialize timestep}
2: while  $\neg succeed$  do
3:    $I_t \leftarrow 1280 \times 720 \times 6$  raw stereo camera image
4:    $s_t \leftarrow$  left, right robot kinematics states
5:    $i_t \leftarrow \text{resize}(I_t, (128, 72))$  {resized stereo global image}

6:    $g_t \leftarrow \rho(i_t)$  {predicted gaze position}
7:    $o_t \leftarrow \text{crop}(I_t, g_t)$  {crop stereo foveated vision}
8:   if  $ATC(o_t)$  is global then
9:      $s_{t+1}, s_{t+2}, \dots, s_T \leftarrow \pi_{global}(o_t, s_t, g_t)$ 
10:     $t' \leftarrow t$ 
11:    while  $ATC(o_t)$  is global do
12:      Execute  $s_{t'}$  on robot
13:       $t' \leftarrow t' + 1$ 
14:    end while
15:     $t \leftarrow t'$ 
16:  else
17:     $a_t \leftarrow \pi_{local}(o_t)$  {local action}
18:    Execute  $a_t$  on robot
19:     $t \leftarrow t + 1$ 
20:  end if
21:   $succeed \leftarrow$  subtask success classifier {manual decision or automated (see IV-F)}
22: end while

```

the end-effector [3]. In this architecture, information about the global coordinate is lost, and the neural network only focuses on the relationship between the target object and the end-effector. Therefore, this network predicts and uses the goal state in a modified form; the relative goal state $s_T^{local} = s_T - s_t = \pi_{local}^{goal}(o_t)$ is inferred and used to predict the reactive action, where π_{local}^{goal} is goal predictor of the local-action network. Therefore, the reactive action is conditioned by current foveated visual information and relative goal state: $a_t = s_{t+1} - s_t = \pi_{local}^{policy}(o_t, s_T^{local})$, where π_{local}^{policy} refers to the policy inference of the local-action network.

D. Model architecture

Figure 3 illustrates the model architecture.

1) *Gaze predictor*: The gaze predictor uses similar models described in [3]. The input 1280×720 raw image is resized into a 128×72 global image then used to predict the gaze coordinate $x_{left}, y_{left}, x_{right}, y_{right}$ measured from the eye tracker while generating the demonstration data. Five consequent convolutional layers and SpatialSoftmax [1] process the global image to predict two-dimensional feature coordinates then passes a mixture density network (MDN) [52], [53] to fit a Gaussian mixture model (GMM) with eight Gaussians into two-dimensional stereo gaze coordinate using the following

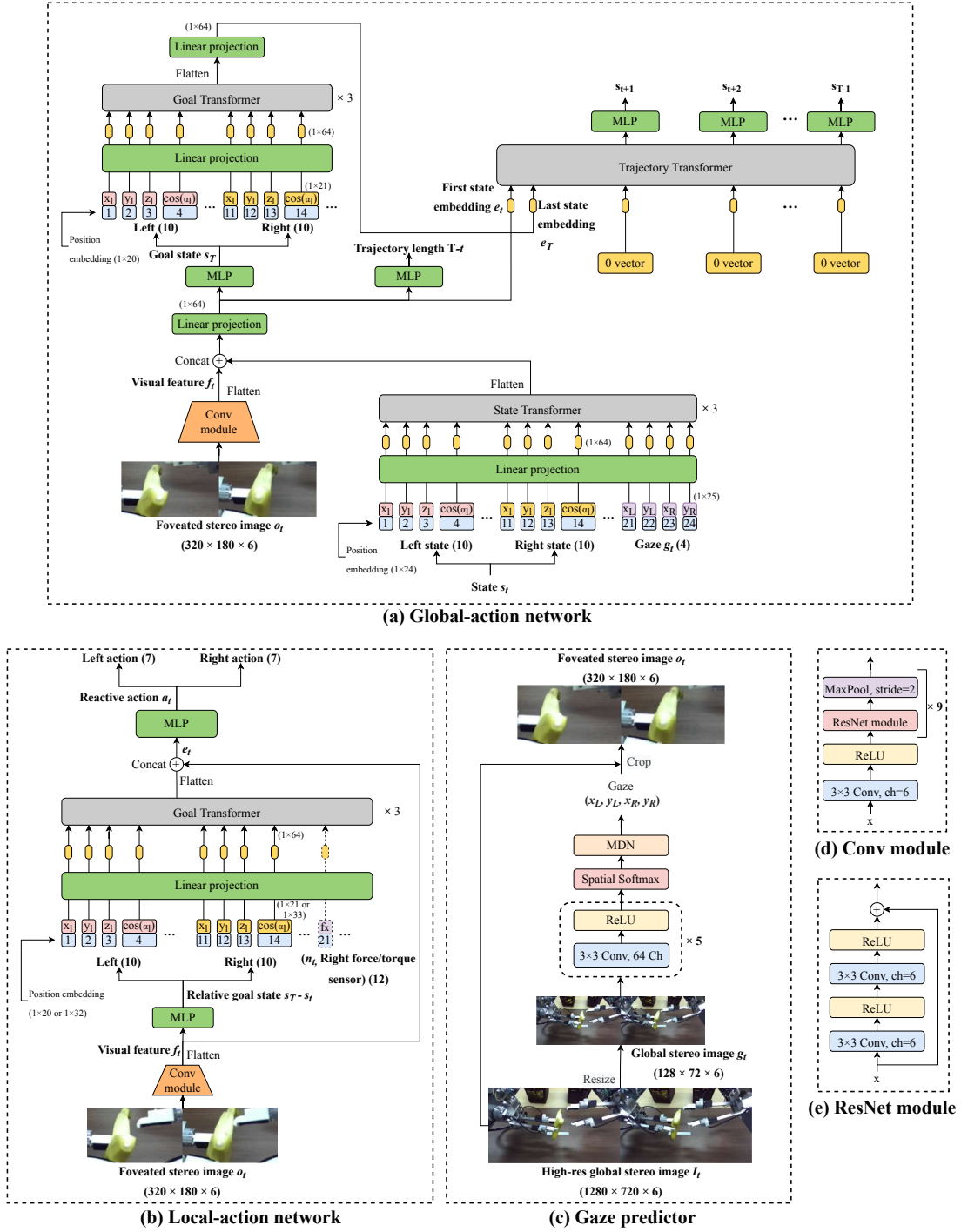


Fig. 3. Detailed neural network architecture of *GC-DA*.

loss:

$$\mathcal{L}_{gaze} = -\log\left(\sum_{i=1}^{N'} w_t^i \mathcal{N}(h_t; \mu_t^i, \Sigma_t^i)\right), \quad (1)$$

where μ_t , Σ_t , w_t indicates the mean, covariance matrix, and the weight of each Gaussian and h_t indicates the measured human gaze during the demonstration. The MDN used two fully connected (FC) layers with rectified linear units (ReLU) between layers.

During the test, the robot chooses a stereo gaze coordinate which maximizes the probability of the GMM. The stereo gaze coordinate is used to crop (stereo) the RGB foveated image (320 × 180 × 6) from the raw stereo image (1280 × 720 × 6).

2) *Local-action network*: Local action outputs reactive action using the foveated image. The input foveated image o_t is processed using residual connections [54] to extract the visual feature f_t using convolutional layers. From this feature, the relative goal state $s_t^{local} = s_T - s_t$ are predicted using MLP.

Based on the results obtained from [4], which demon-

strated that the Transformer-based self-attention mechanism could reduce distractions in high-dimensional somatosensory information, relative goal state is processed using the Transformer encoder architecture (Goal Transformer) to focus on more important features. The output of the Goal Transformer is concatenated with f_t then processed by MLP to output left/right reactive action. For peeling subtasks, the force/torque sensor value of the right hand is also an input to the Goal Transformer so that the robot can also consider the tactile information during peeling.

3) *Global-action network*: The global-action network also inputs o_t to extract visual features f_t using the same ResNet-based architecture described in III-D2. At this time, because the end-effector is usually out of the foveated vision, the left/right robot state and the gaze position are processed with the Transformer encoder (State Transformer) to minimize distraction. e_t , which is a linearly-projected concatenation of f_t and the State Transformer output, passes MLP to predict goal left/right state and a length of the trajectory $T - t$. e_t is considered as the initial embedding of the entire sequence, and the predicted goal state is processed by the Goal Transformer and linearly projected to make the last embedding. $T - t$ zero embeddings are generated to assign space for expected trajectory $s_{t+1}, s_{t+2}, \dots, s_{T-1}$. All embeddings are gathered and processed by another Transformer encoder (Trajectory Transformer) to predict trajectory $s_{t+1}, s_{t+2}, \dots, s_{T-1}$. The robot executes $s_{t+1}, s_{t+2}, \dots, s_{T-1}$ and the inferred goal state s_T sequentially, during $ATC(o_{t' \in \{t+1, \dots, T\}}) = global$.

In every neural network architecture, the Transformer that encodes robot states, gaze, or force/torque sensory input uses learned position embedding that passes linear projection because its length is fixed. Besides, the Trajectory Transformer which generates trajectory action uses sinusoidal positional embedding [55] as it has to process the flexible length of the trajectory.

The MLP is three FC layers with ReLU between FC layers with 200 nodes in each layer. The training minimizes ℓ_2 loss between model output and the ground-truth action. Other model training details are described in Appendix C. Every subtask described in III-B is trained with the separated model.

E. Global/local action separation

The proposed dual-action-based method is composed of global and local action. This dual-action-based method requires separating the local action from the demonstration subtask sequence. For example, on a demonstration sequence with timesteps $\{0, 1, 2, \dots, T\}$, steps between $[t_1, t_2]$ are annotated as the local action, where t_1 and t_2 are determined from a criterion that decides local action. The entire timesteps $\{0, 1, 2, \dots, T\}$ are considered as the global action.

This subsection explains the separation criteria on reach and peeling subtasks, based on a basic criterion that reactive action is selected when the precise manipulation is required. Note that this action separation does not change the definition of the goal state; even after the separation, global and local actions share the same goal state s_T .

1) *Reach subtasks*: The step is annotated as local action in reaching subtasks if the end-effector is in the foveated image (Fig. 13) because in reaching to the target, precise manipulation is required at the end of the sequence that tries the last-inch reaching to the exact location of the target [3], [56]. Because the reaching subtasks contain lots of demonstrations (> 2140 , Table II), a CNN-based classifier trained with a small amount of human-annotated data is used to annotate the entire dataset. The details of the automated annotation method can be found in Appendix B. The action-type classifier (ATC) is trained based on the annotated labels if the end-effector is in the foveated vision.

2) *Peel subtasks*: In *PeelTip*, the criterion is if the tip of the banana is peeled (Appendix A) because a force feedback-based high-precision reactive control is required to tear the tip without severely damage to the banana. After it is torn, no force feedback or highly precise reaching to the goal is required. All demonstrations are annotated manually as the dataset is comparatively small (256 for training and 23 for validation). The annotated data also train another ATC.

In *PeelRight* and *PeelLeft*, the criterion is relatively simple; a step is classified as global-action if the end-effector is closed. In these subtasks, the robot has to control its end-effector precisely with the reactive action during closing so that after complete closure, the end-effector can hold the peel. On the other hand, peeling behavior after the holding requires the simple behavior of pulling the firmly held peel, which does not require high-precision manipulation.

IV. EVALUATION

A. Experiment setup

The banana peeling task is a long-horizon task that consists of 9 subtasks from *GraspBanana* to *PeelLeft*, and each subtask requires the previous subtask to be successful. If all subtasks are conducted consecutively, we can test only a few samples on later subtasks such as *ReachLeft* or *PeelLeft*. Therefore, we tested each subtask by executing the subtask then modifying the banana position so that the robot could execute the next subtask: for example, if the robot fell off the banana, it was placed in the robot's hand again.

To maintain the condition of bananas, we bought bananas in the local market and used on the same day. Each banana was scratched for $1cm$ because even the human operator could not peel the banana through teleoperation because the tip was too stiff to break. We found that the banana became peelable with teleoperation after two days ripened. However, the banana also became soft and easily breakable; controlling the banana condition became difficult.

B. Ablation studies

This paper raises the following questions:

- Is the proposed dual-action system valid?
- Is goal-conditioned action inference effective?

Ablation studies in Table III were scheduled to solve the questions above. (a) *GC-DA* fully utilizes the proposed dual-action architecture and goal-conditioned action inference.

TABLE III
ABLATION STUDY DETAILS.

Method	Action type	Local		Global		
		Goal conditioning	Action type	Goal conditioning	Vision type	
(a) <i>GC-DA</i>	Reactive	✓	Trajectory	✓	Foveated	
(b) <i>NoGC (Global)</i>	Reactive	✓	Trajectory	✗	Foveated	
(c) <i>NoGC (Local)</i>	Reactive	✗	Trajectory	✓	Foveated	
(d) <i>NoGC (Both)</i>	Reactive	✗	Trajectory	✗	Foveated	
(e) <i>Reactive</i>	Reactive	✓	Reactive	✓	Foveated	
(f) <i>Reactive-NoGC</i>	Reactive	✗	Reactive	✗	Foveated	
(g) <i>Traj</i>	Trajectory	✓	Trajectory	✓	Foveated	
(h) <i>Dual-resolution</i>	Reactive	✓	Trajectory	✓	Global	

TABLE IV
RESULTS OF THE ABLATION STUDIES.

Method	<i>GraspBanana</i>	<i>GraspTip</i>	<i>PeelTip</i>	<i>ReachRight</i>	<i>PeelRight</i>	<i>ReachLeft</i>	<i>PeelLeft</i>	Mean
(a) <i>GC-DA</i>	1.000	0.933	0.833	0.933	0.750	0.846	0.792	0.870
(b) <i>NoGC (Global)</i>	0.867	0.667	0.633	0.692	0.679	0.533	0.833	0.701
(c) <i>NoGC (Local)</i>	1.000	0.867	0.600	0.667	0.893	0.462	0.667	0.736
(d) <i>NoGC (Both)</i>	1.000	0.800	0.200	0.467	0.643	0.800	0.731	0.663
(e) <i>Reactive</i>	0.867	0.400	0.800	0.583	0.708	0.700	0.778	0.691
(f) <i>Reactive-NoGC</i>	1.000	0.600	0.929	0.600	0.667	0.692	0.792	0.754
(g) <i>Traj</i>	1.000	0.000	0.833	0.000	0.571	0.231	N/A	0.439
(h) <i>Dual-resolution</i>	1.000	0.600	0.700	0.500	0.775	0.714	0.607	0.696

NoGCs ((b) ~ (d)) do not use the goal-conditioned action inference on global action (b), local action (c), and both (d). (e) *Reactive* examines the performance of reactive global action. (f) *Reactive-NoGC* combines (d) *NoGC (both)* and (e) *Reactive*; global/local actions are not conditioned by goal state and are reactive. Opposite to (e), in (g) *Traj*, both global/local actions are trajectory. To evaluate the combination of global action with global vision proposed in [3], (h) *Dual-resolution* tested trajectory-based global action inferred from the global image. In (h), the global image was processed by five consequent convolutional layers combined with SpatialSoftmax [3], [12].

C. Experiment result

Each ablation study was tested with 15 bananas. Details of evaluation criteria are explained in Appendix D.

Table IV demonstrates the experiment results. *PickUp* and *Reposition* were not evaluated because these subtasks are intermediate behaviors that connect the previous subtask to the next subtask; therefore, the evaluation metric is ambiguous. The proposed *GC-DA* recorded the highest mean score. Remarkably, the *GC-DA* scored highest in all reaching subtasks. Some ablation studies without the goal-conditioning ((b), (c)) recorded higher scores in *PeelRight* and *PeelLeft*, respectively, but all ablation studies without *GC* ((b) ~ (d)) recorded lower accuracy in reaching subtasks. This result infers that goal-conditioned action inference improves manipulation accuracy during precise reaching. On the other hand, inferring the exact goal position is not essential for peeling subtasks.

When the global-action network output reactive instead of trajectory ((e) ~ (f)) and the local action predicted trajectory (g), performance dropped on reaching subtasks. These results

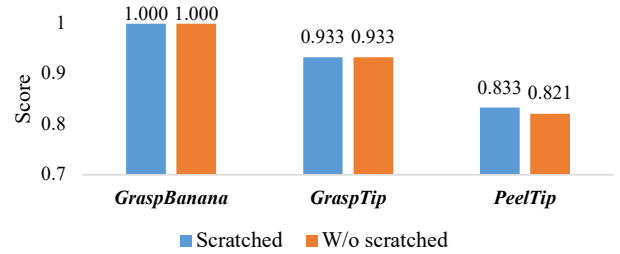


Fig. 4. Scores until *PeelTip* for experiments using the scratched bananas (blue) and the two-days-ripped bananas without the scratch (orange). The result indicates that there is no difference between the two.

also show that the combination of reactive local action and trajectory-based global action is essential.

The result in (h) *Dual-resolution* indicates dual-resolution architecture where the global action is computed from global vision deters the reaching performance. In our previous research adopted dual-resolution architecture [3], two-dimensional translation of end-effector was required for global action, was sufficient with the low-resolution global vision. However, in the banana peeling task, during global action, the robot has to calculate a robust, exact three-dimensional trajectory to the vicinity of banana peels, which requires the high-resolution foveated vision for depth computation and suppression of background distractions [12].

Figure 4 illustrates the manipulation score until *PeelTip* of both scratched bananas (Table IV (a)) and bananas ripened for two days without the scratch. Both showed similar scores, indicating that the banana can be peeled without the scratch with enough ripening.

TABLE V
MEAN (\pm STD) OF EUCLADIAN DISTANCE ERROR BETWEEN s_1 AND s_0
IN FIG. 5: $\|s_1 - s_0\|$.

Reactive (mm)	Trajectory (mm)
23.8 ± 3.67	34.8 ± 5.71

D. Analysis on trajectory inference

This subsection analyzed why trajectory-based global action outperforms reactive global action. First, Fig. 5 investigated the routes between trajectory-based global action and reactive global action. For the test data collected using (e) *Reactive*, the *GraspTip* subtask’s positional relative route against the initial position s_0 of the global action and re-computed trajectory-based global action is plotted. The result indicates that the reactive and trajectory-based actions show different routes. Mainly, the first trajectory-based global action state s_1 is apart more from the initial position s_0 than reactive action’s s_1 (Table V).

Second, the Transformer’s attention analysis indicates that the trajectory-based action inference is conditioned more on goal state than reactive action; therefore, the policy is more stable. Figure 6 computed attentions on both trajectory-based global action and reactive global action¹. These attention maps were computed by averaging attention rollout [57] of the Transformer’s attention weights in embeddings s_t , s_T , and $[s_{t+1}, \dots, s_{T-1}]$, respectively. The result clearly shows that the generated trajectories (target: $[s_{t+1}, \dots, s_{T-1}]$) are heavily conditioned on the inferred goal state (source: s_T , Fig 6a). On the other hand, Fig. 6b indicates that the reactive global action is heavily conditioned on current robot kinematic state s_t and less on goal state s_T (see Appendix F for details of attention computation).

Considering the results in Fig. 5, Table V, and Fig. 6a, trajectory-based global action is less conditioned by initial position but goal state; s_1 is less related to initial state s_0 . Besides, the first reactive global action, which is defined by $a_1 = s_1 - s_0$ is heavily conditioned by initial position s_0 . Therefore, s_1 is in the vicinity of s_0 . To sum up, the trajectory-based global action is more conditioned to the goal state than reactive global action, therefore outputs constant routes toward the goal regardless of initial robot kinematic states.

E. Analysis on the goal-conditioning

This subsection analyzes the necessity of goal conditioning typically during reach subtasks. Figure 7 visualizes the accuracy of goal state inference on the validation set. In this figure, the mean Euclid distance between the ground-truth goal state and the predicted goal state of the right arm computed by the global-action network for every timestep is computed. The Euclid error is low ($< 11mm$) for reach subtasks (blue) but high for peeling subtasks (orange). This result indicates that peeling subtasks are less conditioned by goal state; i.e., peeling

¹Unlike the (e) *Reactive* in Table III and IV, the network trained at this time the Transformer mechanism also input current state s_t , gaze position g_t , and visual feature o_t .

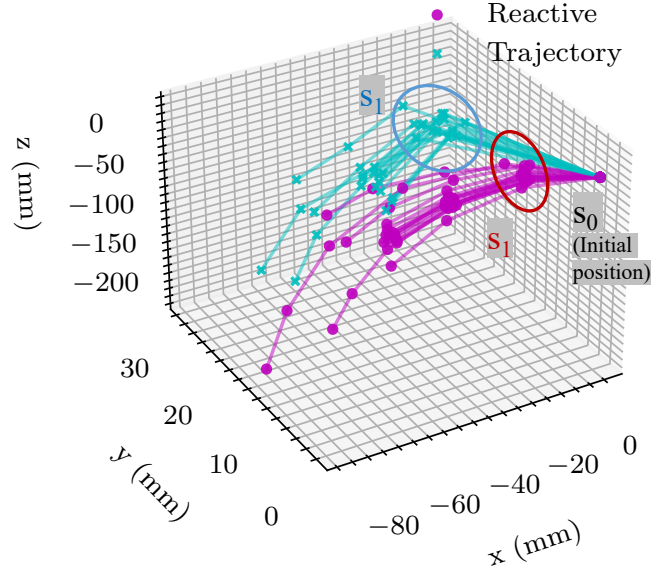
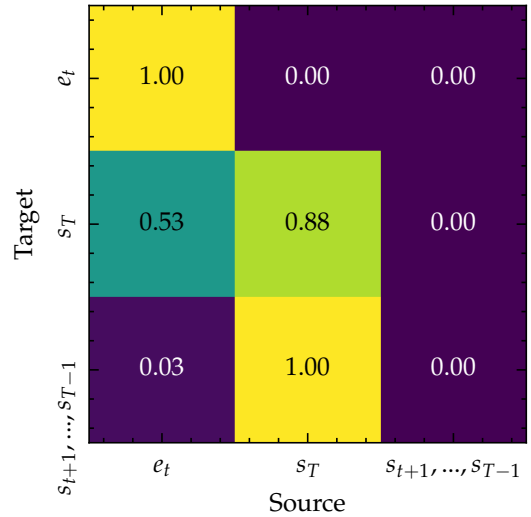
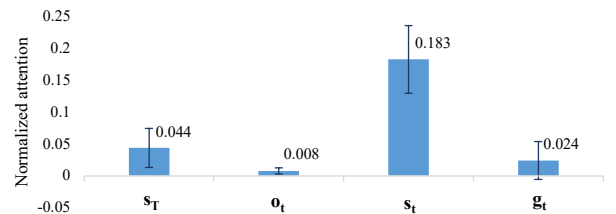


Fig. 5. Routes of trajectory-based and reactive actions on *GraspTip*.



(a) Attention map of trajectory-based global action.



(b) Attention of reactive global action.

Fig. 6. Attentions on trajectory-based and reactive global actions. The trajectory s_{t+1}, \dots, s_{T-1} attended on the goal state s_T (Fig. 6a) while reactive global action attended more on initial state s_t (6b).

can be ended anywhere after the peel is torn but reaching needs to be ended at the exact location at the banana peel or tip. The above result supports the result in Table IV (b) and (c), where non-goal-conditioned (*NoGC*) models sometimes

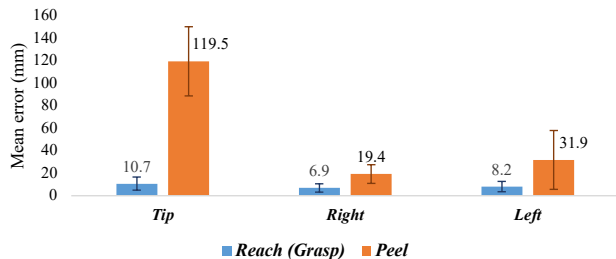


Fig. 7. Error comparisons of goal state prediction in reach and peel subtasks by global-action networks.

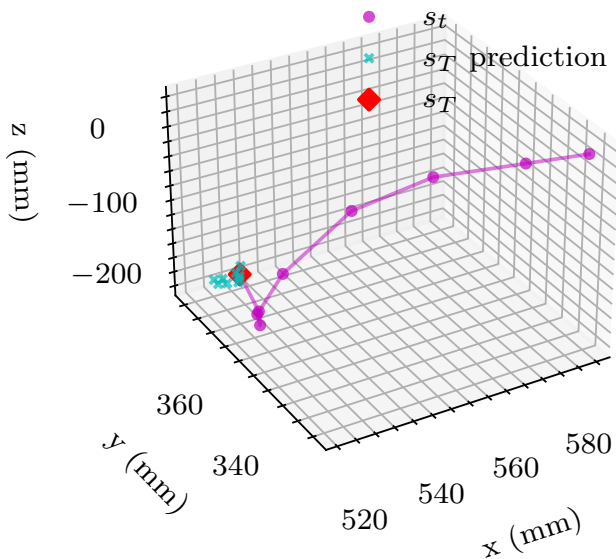


Fig. 8. Example recorded trajectory and the predicted goal states in *ReachTip* visualized. s_T prediction indicates the predicted goal state s_T from every state s_t .

showed higher peeling scores than *GC-DA*, as peeling subtasks less require goal conditioned action inference. Also, even though goal prediction accuracy of $< 11\text{mm}$ is enough for many pick-and-place tasks, this is not sufficient for reach the peel in our task setup; therefore, recursive last-inch reaching is required.

Figure 8 visualizes a recorded trajectory s_0, \dots, s_T in an episode in the validation set of *ReachTip* and the predicted goal state s_T from each state $s_t, t \in [0, T)$. The goal state can be predicted regardless of the current state s_t .

F. Consecutive banana peeling

This section describes the experimental setup and results of consecutive banana peeling. In this setup, the robot peels the banana from start (*GraspBanana*) to end (*PeelLeft*) without human intervention.

1) *Methods for consecutive banana peeling setup*: We found that the banana slipped from the robot hand during consecutive banana peeling. To prevent this, we designed the following methods. First, an attachment to the left end-effector supports the banana to not tilt during peeling (see Fig. 9,

11). Second, a behavior that pushes the banana tip 30mm to the left was adopted to prevent the banana from tilting (Fig. 9, 22s ~ 30s). Finally, after *PeelTip*, the banana posture is rearranged before executing *ReachRight*. This behavior is conducted using a simple neural network architecture trained to infer the *PeelTip*'s goal robot posture from all *ReachRight*'s initial states. This architecture ensures to drive the initial state of *ReachRight* to be in the state distribution of the training dataset (Fig. 10).

2) *Transition between subtasks*: There are two different types of transitions between adjacent subtasks. First, when the earlier subtask is ended with trajectory inference (*GraspBanana*, *PickUp*, *Reposition*), and Peel subtasks when trajectory-based global action is used for peeling (IV-F3), later subtask can be conducted as soon as the current trajectory execution is done. Otherwise, if the subtask ends with reactive action (reach subtasks and peel subtasks if peel subtasks use reactive global action), the transition between subtasks requires additional classifiers.

The robot changes *GraspTip* to *PeelTip* when the right end-effector is closed. *ReachLeft* and *ReachRight* use additional CNN-based classifiers (next subsection classifier, NSC). In *ReachRight*, the NSC is trained with classified foveated images in *ReachRight* and *PeelRight*; if the current foveated image o_t is classified as *PeelRight*, the subtask to execute is shifted to *PeelRight*. In *ReachLeft*, another NSC also classifies foveated images in *ReachLeft* and *PeelLeft*. The NSC comprises the Conv module described in Fig. 3 (d) and three-layer MLP.

3) *Reactive peeling vs Trajectory-based peeling*: The comparison between Table IV (a) *GC-DA* and (e) *Reactive* indicates there are little difference in peeling scores. To double-check it in a consecutive banana peeling setup, we compared the proposed *GC-DA* with a model that replaced trajectory-based global action with reactive global action for peeling subtasks. In reactive peeling, peeling subtasks use trained NCS between current peeling subtask and next subtask. Figure 12 illustrates the mean (11 bananas) cumulative product of score of *GC-DA* with trajectory-based global action and reactive global action for peeling in consecutive peeling setup, which indicates there is little difference in the final score (0.575 vs. 0.544).

4) *Example trials*: Figure 9 illustrates the successful behavior of *GC-DA* with reactive global action for peeling on the consecutive banana peeling setup. On the other hand, Fig. 11 shows failure examples in the same setup, including the robot destroying the banana (Fig. 11a) and the robot slipping the banana (Fig. 11b).

V. CONCLUSION

This paper realized the banana peeling task with a general-purpose dual-arm robot based on the proposed goal-conditioned dual-action (*GC-DA*) deep imitation learning. The proposed method separates the policy of robot motion into global and local action. A trajectory-based global action is used to deliver the end-effector stably to near the goal position when the robot less requires the precise manipulation of the target object, such as delivering the robot arm in the vicinity to

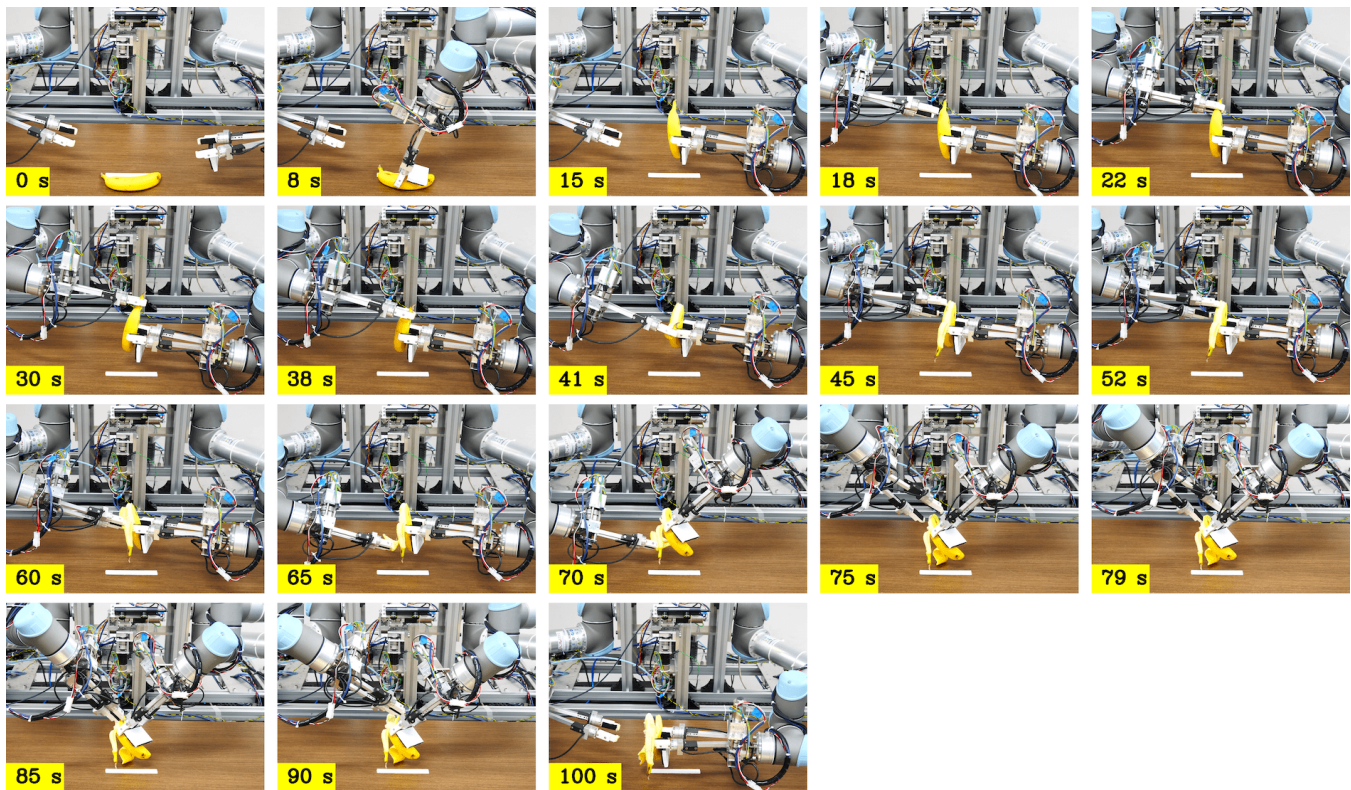


Fig. 9. Example successful trial. The robot grasped and picked up the banana ($\sim 15s$), reached its right end-effector to the tip ($\sim 22s$), pushed it for $30mm$ left for additional stability ($30s$), then peeled the tip ($38 \sim 41s$). Then, the robot reached its right end-effector to the right side of the banana and peeled it ($45 \sim 65s$). Finally, the robot rotated the banana ($70s$) and peeled the left part ($75 \sim 100s$).

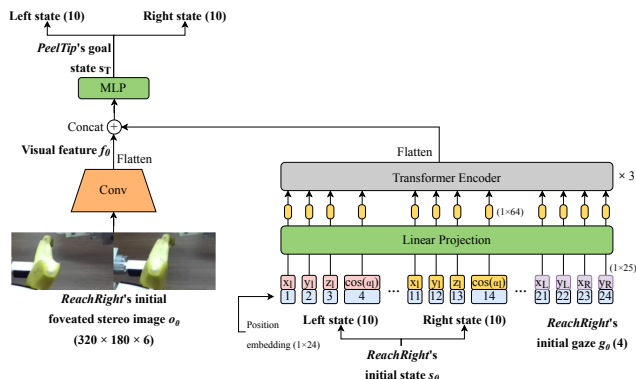


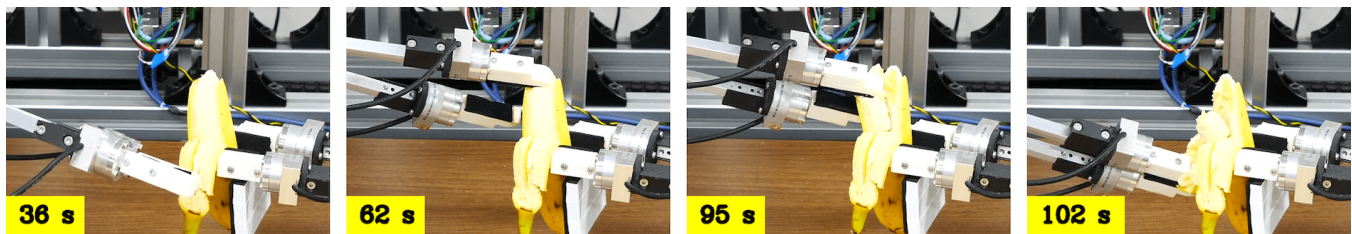
Fig. 10. *Rearrange* network architecture.

the banana peel. The reactive local action precisely controls the end-effector to manipulate the target object, such as the precise last-inch reaching to the banana peel. The inferred goal state conditions the model's output action for stable policy inference. The proposed *GC-DA* successfully peeled the real banana using a dual-arm manipulator. This result is important for two reasons: first, highly dexterous, long-horizon robot manipulation of deformable object, is possible without the task-specific gripper. Second, The above dexterous manipulation skills were acquired from only human-generated behavior data, without pre-defined manipulation rules. Therefore, the proposed method is not limited to the banana peeling task

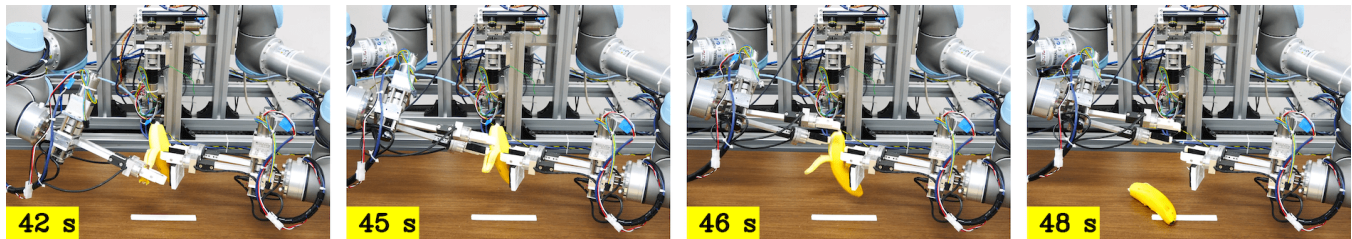
but can be applied to other robot manipulation tasks requiring dexterity.

The experiments compared reactive global action and trajectory-based global action (Table IV (e), (f), Fig. 12) indicate that during peeling subtasks, reactive global action and trajectory-based global action recorded similar performances. In the peeling subtasks, the global/local action segmentation criterion is not depend on if the end-effector is in the foveated image (Appendix A). This result about peeling performances supports that the segmentation between trajectory-based global action and reactive local action only depend on the existence of the end-effector in the foveated image. Therefore, autonomous global/local action segmentation based on the criterion of the existence of the end-effector in the foveated image can be built and be generally used for various tasks and environments.

In this research, 811 minutes ≈ 13.5 hours of demonstration data were generated and trained, which can be obtained in only a few days. Considering the complexity of the target banana peeling task, we think 13.h hours of demonstration is feasible. However, data efficiency has always been pursued on learning-based robotics. Therefore, our future interest is to study if few-shot learning of highly dexterous manipulation skills is possible with transferring knowledge of objects and behaviors. Previously, the importance of behavior segmentation and structured behavior and tasks have been reported [31], [58], [59]. Because the unsupervised segmentation is possible with gaze [60] and the gaze information is highly correlated with task objective [61], [62], we hypothesize that gaze can be



(a) The robot destroyed the banana because it did not reach the exact location (62s) and tried to peel, destroying the banana.



(b) The banana was slipped from the robot's hand.

Fig. 11. Failure examples of banana peeling.

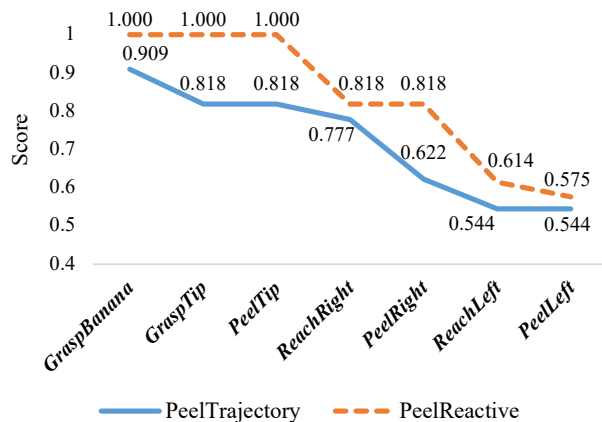


Fig. 12. Cumulative product of score for consecutive peeling setup in PeelTrajectory (Trajectory-based global action for peeling subtasks) and PeelReactive (Reactive global action for peeling subtasks).

applied to unsupervised segmentation and structuring of tasks and further be applied to transfer of behavior to other tasks. The application of gaze-based human behavior segmentation for structured deep imitation learning is a promising topic for future research.

APPENDIX

A. Boundaries between global/local actions in reaching subtasks

Figure 13 illustrates examples of boundaries between global and local actions in each subtask. In reaching subtasks, a step is identified as local action if the effective end-effector is in the foveated image (Fig. 13a, 13c, 13e). In *PeelTip* (Fig. 13b), a behavior that opens the banana tip is identified as local action, and peeling behavior is identified as the global action. In *PeelLeft* (Fig. 13d) and *PeelRight* (Fig. 13f), grasping the banana peel is defined as local action, and peeling behavior is identified as global action.

TABLE VI

NUMBER OF ANNOTATED, CLASSIFIED BY THE TRAINED MODEL, AND RE-ANNOTATED DEMONSTRATIONS ON EACH SUBTASK.

Subtask	# of annotated	# of classified	# of re-annotated
<i>GraspTip</i>	283	2087	369
<i>ReachRight</i>	400	4546	288
<i>ReachLeft</i>	400	4065	202

B. Annotation method

To reduce the time required for annotation, we used an image classifier for automated annotation similar to [63]'s. First, a human manually annotates part of the entire episode into global/local action. For example, the human annotated 283 episodes from the entire 2370 episodes in *GraspTip* subtask. Then, a simple CNN-based image classifier is trained using the annotated dataset (90% training, 10% validation). This CNN-based classifier comprises ten consecutive convolutional layers with ReLU, and maxpooling is between every two convolutional layers. The output of convolutional layers is passed through two layers of MLP and returns binary classification results: $C(o_t) \rightarrow \{global\ action, local\ action\}$, where C indicates the trained classifier. Next, the trained classifier annotates the unannotated episodes. To filter false classification results, we utilized the fact that the transition between global and local action occurs only once. On reaching subtasks, if $C(o_t) \rightarrow local\ action$ and $C(o_{t+1}) \rightarrow global\ action$ for any t in the timestep $0, \dots, T-1$ in an episode with length T , this episode is re-annotated by the human. On peeling subtasks, human re-annotated episodes with $C(o_t) \rightarrow global\ action$ and $C(o_{t+1}) \rightarrow local\ action$. Table VI represents the number of demonstrations annotated by humans used for the model training, classified demonstrations by the trained model, and the re-annotated demonstrations.

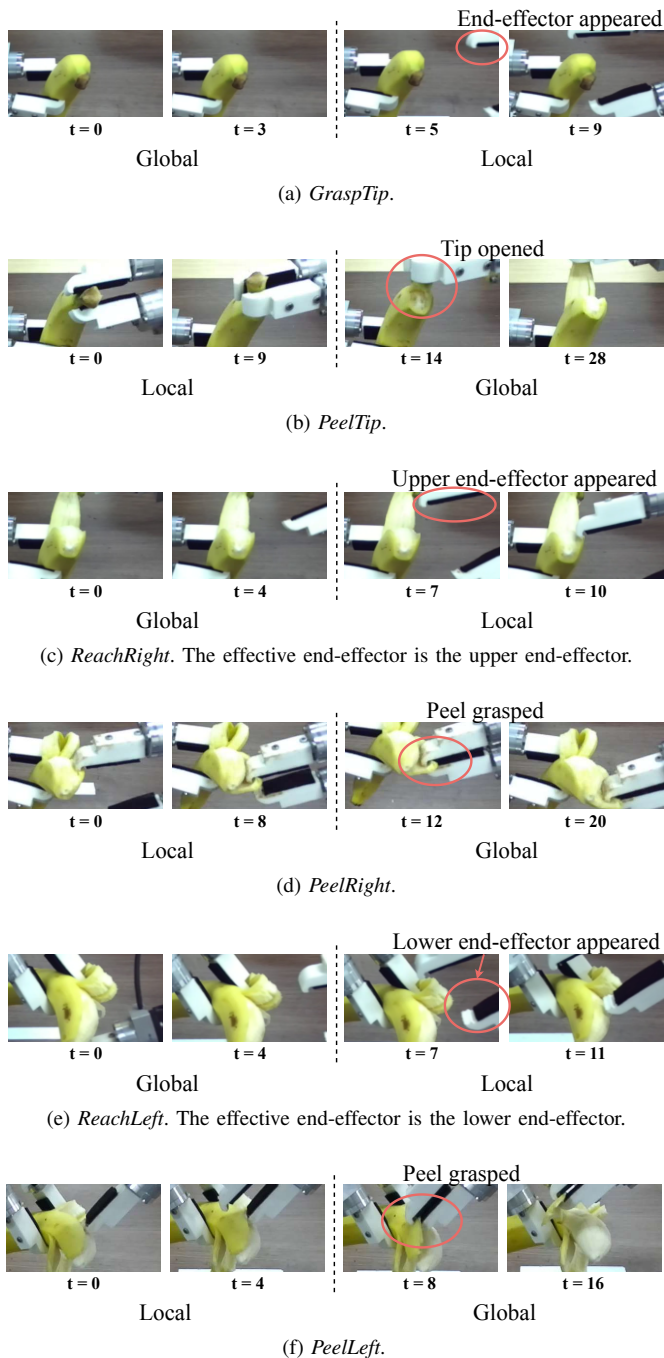


Fig. 13. Boundaries displayed in foveated image.

C. Model training details

This research follows model training details as described in [50]. A rectified Adam optimizer [64] with learning rate of $3e - 5$, weight decay of 0.01, and batch size of 16 were used to train the proposed model. Two AMP EPYC 7402 CPUs with four NVIDIA a100 and Intel Xeon CPU E5-2609 v4 with eight NVIDIA v100 GPUs were used for training the model. Because reaching subtasks are more complex than other subtasks, they were trained for 500 epochs, and other subtasks were trained for 300 epochs. During execution on the robot, Intel CPU Core i7-8700K and one NVIDIA GeForce

GTX 1080 Ti were used.

D. Scoring criteria

The model was scored +1 if it achieved the objective of each subtask and +0 if it did not. In addition, on peeling subtasks, specific scoring criteria were set because peeled state is iffy:

- *PeelTip*: +0.5 for opening the tip and +1 for entirely peeling the tip.
- *PeelRight*: If the bottom side of the peel is still attached, scored +0.5. If it is entirely torn, scored +1.
- *PeelLeft*: If the bottom side of the peel is still attached, scored +0.5. If it is entirely torn, scored +1.

Figure 14 visualizes examples of those criteria.

E. Data augmentation

Image augmentation is often used in computer vision to increase the robustness of the neural network against input data. This research randomly adjusted brightness, contrast, saturation, and hue to transform the training input images. Additionally, random erasing [65] is applied to prevent overfitting of the neural network model to the specific features only exist in training data.

F. Attention computation

The computation of the attention map follows [63]. The trajectory-based global-action network inputs current state embedding e_t , inferred goal state s_T , and zero vectors s_{t+1}, \dots, s_{T-1} . On this input sequence, attention rollout [57] $A^{\{T-t+1\} \times \{T-t+1\}}$ defined by the recursive multiplication of attention weight of each layer in the trajectory Transformer is computed. To normalize the attention rollout on each target embedding, the attention rollout is divided by the maximum of target embedding values:

$$M_{i,j} = \frac{A_{i,j}}{\max(A_i)}, \quad (2)$$

where $i \in [0, T)$, $j \in [0, T)$ and M is the sequential attention map. Then, attention on zero vectors s_{t+1}, \dots, s_{T-1} are averaged. The output attention map size is 3×3 where elements indicates $[e_t, s_T, \{s_t + 1, \dots, s_T - 1\}]$.

Similarly, the eq. 2 normalized an attention rollout of reactive global-action network output. The Transformer output embeddings of the reactive global-action network are flattened and pass MLP to compute the a_t . Therefore, the information of which source embedding is attended to is more important than the attention map that considers the target embedding. The summation of target embedding corresponding to o_t, s_t, g_t , and s_T are computed by following:

$$W^{s_T} = \sum_{i=0}^{138} \sum_{j=0}^{19} A_{ij}, \quad (3)$$

$$W^{o_t} = \sum_{i=0}^{138} \sum_{j=20}^{114} A_{ij}, \quad (4)$$

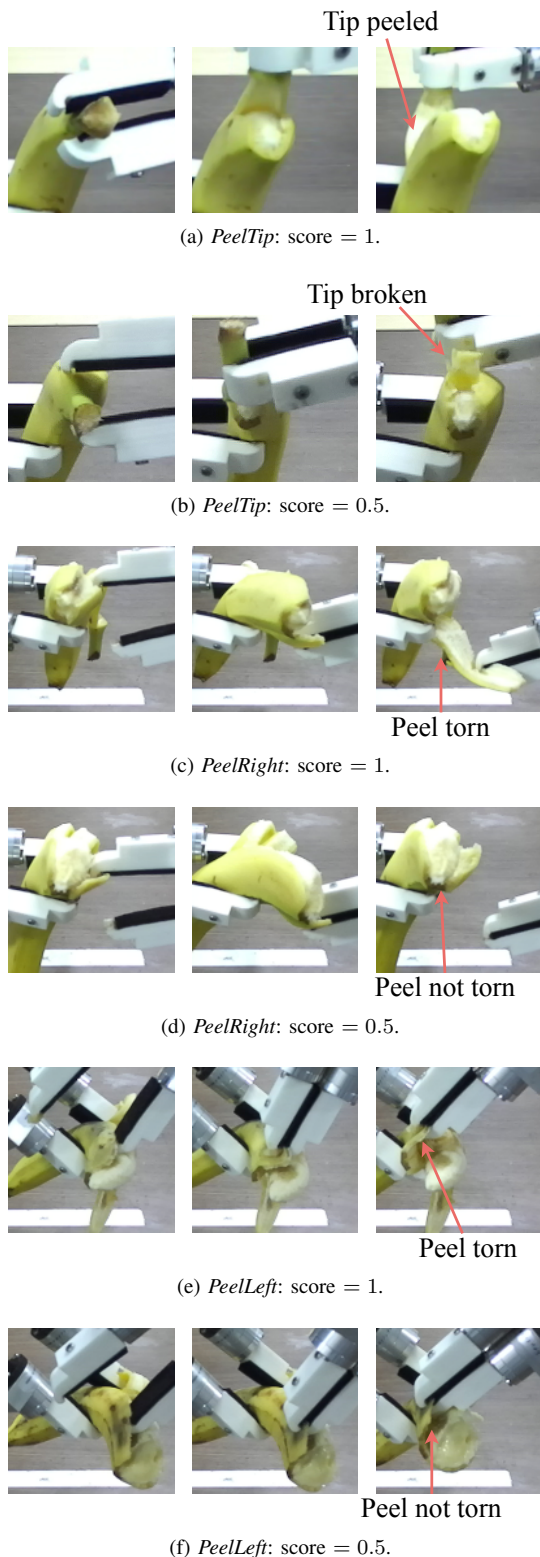


Fig. 14. Examples of criteria.

$$W^{st} = \sum_{i=0}^{138} \sum_{j=115}^{134} A_{ij}, \quad (5)$$

$$W^{gt} = \sum_{i=0}^{138} \sum_{j=135}^{138} A_{ij}. \quad (6)$$

ACKNOWLEDGMENTS

This paper is supported in part by the Department of Social Cooperation Program “Intelligent Mobility Society Design,” funded by Toyota Central R&D Labs., Inc., of the Next Generation AI Research Center, The University of Tokyo.

REFERENCES

- [1] C. Finn, X. Y. Tan, Y. Duan, T. Darrell, S. Levine, and P. Abbeel, “Deep spatial autoencoders for visuomotor learning,” in *International Conference on Robotics and Automation*, 2016, pp. 512–519.
- [2] T. Zhang, Z. McCarthy, O. Jow, D. Lee, X. Chen, K. Goldberg, and P. Abbeel, “Deep imitation learning for complex manipulation tasks from virtual reality teleoperation,” in *International Conference on Robotics and Automation*, 2018, pp. 1–8.
- [3] H. Kim, Y. Ohmura, and Y. Kuniyoshi, “Gaze-based dual resolution deep imitation learning for high-precision dexterous robot manipulation,” *Robotics and Automation Letters*, vol. 6, no. 2, pp. 1630–1637, 2021.
- [4] H. Kim, Y. Ohmura, and Y. Kuniyoshi, “Transformer-based deep imitation learning for dual-arm robot manipulation,” in *International Conference on Intelligent Robots and Systems*, 2021.
- [5] L. Manuelli, W. Gao, P. Florence, and R. Tedrake, “kpm: Keypoint affordances for category-level robotic manipulation,” in *International Symposium on Robotics Research*, 2019.
- [6] J. Mahler, M. Matl, V. Satish, M. Danielczuk, B. DeRose, S. McKinley, and K. Goldberg, “Learning ambidextrous robot grasping policies,” *Science Robotics*, vol. 4, no. 26, p. eaau4984, 2019.
- [7] J. Wang, S. Lin, C. Hu, Y. Zhu, and L. Zhu, “Learning semantic keypoint representations for door opening manipulation,” *IEEE Robotics and Automation Letters*, vol. 5, no. 4, pp. 6980–6987, 2020.
- [8] E. Y. Puang, K. P. Tee, and W. Jing, “Kovis: Keypoint-based visual servoing with zero-shot sim-to-real transfer for robotics manipulation,” in *International Conference on Intelligent Robots and Systems*, 2020, pp. 7527–7533.
- [9] R. Xu, F.-J. Chu, C. Tang, W. Liu, and P. A. Vela, “An affordance keypoint detection network for robot manipulation,” *IEEE Robotics and Automation Letters*, vol. 6, no. 2, pp. 2870–2877, 2021.
- [10] M. Andrychowicz, F. Wolski, A. Ray, J. Schneider, R. Fong, P. Welinder, B. McGrew, J. Tobin, O. P. Abbeel, and W. Zaremba, “Hindsight experience replay,” in *Advances in Neural Information Processing Systems*, 2017, pp. 5048–5058.
- [11] OpenAI, I. Akkaya, M. Andrychowicz, M. Chociej, M. Litwin, B. McGrew, A. Petron, A. Paino, M. Plappert, G. Powell, R. Ribas, J. Schneider, N. Tezak, J. Tworek, P. Welinder, L. Weng, Q. Yuan, W. Zaremba, and L. Zhang, “Solving rubik’s cube with a robot hand,” *arXiv preprint*, 2019.
- [12] H. Kim, Y. Ohmura, and Y. Kuniyoshi, “Using human gaze to improve robustness against irrelevant objects in robot manipulation tasks,” *Robotics and Automation Letters*, vol. 5, no. 3, pp. 4415–4422, 2020.
- [13] D. Koert, G. Maeda, R. Lioutikov, G. Neumann, and J. Peters, “Demonstration based trajectory optimization for generalizable robot motions,” in *International Conference on Humanoid Robots*, 2016, pp. 515–522.
- [14] A. Vakanski, I. Mantegh, A. Irish, and F. Janabi-Sharifi, “Trajectory learning for robot programming by demonstration using hidden markov model and dynamic time warping,” *Transactions on Systems, Man, and Cybernetics*, vol. 42, no. 4, pp. 1039–1052, 2012.
- [15] H. Kim, M. Yamada, K. Miyoshi, T. Iwata, and H. Yamakawa, “Reinforcement learning in latent action sequence space,” in *International Conference on Intelligent Robots and Systems*, 2020, pp. 5497–5503.
- [16] M. Yamada, H. Kim, K. Miyoshi, T. Iwata, and H. Yamakawa, “Disentangled representations for sequence data using information bottleneck principle,” in *Asian Conference on Machine Learning*, 2020, pp. 305–320.
- [17] M. Turpin, K. Mohta, N. Michael, and V. Kumar, “Goal assignment and trajectory planning for large teams of interchangeable robots,” *Autonomous Robots*, vol. 37, no. 4, pp. 401–415, 2014.
- [18] S. Bhattacharya, R. Ghrist, and V. Kumar, “Persistent homology for path planning in uncertain environments,” *IEEE Transactions on Robotics*, vol. 31, no. 3, pp. 578–590, 2015.
- [19] W. Van Loock, G. Pipeleers, M. Diehl, J. De Schutter, and J. Swevers, “Optimal path following for differentially flat robotic systems through a geometric problem formulation,” *IEEE Transactions on Robotics*, vol. 30, no. 4, pp. 980–985, 2014.

- [20] J. D. Gammell, S. S. Srinivasa, and T. D. Barfoot, "Batch informed trees (bit*): Sampling-based optimal planning via the heuristically guided search of implicit random geometric graphs," in *International Conference on Robotics and Automation*, 2015, pp. 3067–3074.
- [21] O. Khatib, "Real-time obstacle avoidance for manipulators and mobile robots," in *Autonomous robot vehicles*, 1986, pp. 396–404.
- [22] Y. K. Hwang, N. Ahuja, et al., "A potential field approach to path planning," *IEEE Transactions on Robotics and Automation*, vol. 8, no. 1, pp. 23–32, 1992.
- [23] K. H. Sedighi, K. Ashenayi, T. W. Manikas, R. L. Wainwright, and H.-M. Tai, "Autonomous local path planning for a mobile robot using a genetic algorithm," in *Congress on Evolutionary Computation*, vol. 2, 2004, pp. 1338–1345.
- [24] K. Cole and A. M. Wickenheiser, "Reactive trajectory generation in an unknown environment," in *International Conference on Intelligent Robots and Systems*, 2017, pp. 2151–2157.
- [25] R. A. Knepper, S. S. Srinivasa, and M. T. Mason, "Hierarchical planning architectures for mobile manipulation tasks in indoor environments," in *International Conference on Robotics and Automation*, 2010, pp. 1985–1990.
- [26] Y. Ding, C. Florensa, P. Abbeel, and M. Phielipp, "Goal-conditioned imitation learning," in *Advances in neural information processing systems*, vol. 32, 2019.
- [27] Y. Lee, A. Szot, S.-H. Sun, and J. J. Lim, "Generalizable imitation learning from observation via inferring goal proximity," in *Advances in Neural Information Processing Systems*, vol. 34, 2021.
- [28] J. Ho and S. Ermon, "Generative adversarial imitation learning," in *Advances in Neural Information Processing Systems*, 2016, pp. 4565–4573.
- [29] I. Goodfellow, J. Pouget-Abadie, M. Mirza, B. Xu, D. Warde-Farley, S. Ozair, A. Courville, and Y. Bengio, "Generative adversarial nets," in *Advances in Neural Information Processing Systems*, 2014, pp. 2672–2680.
- [30] Z. Sui, L. Xiang, O. C. Jenkins, and K. Desingh, "Goal-directed robot manipulation through axiomatic scene estimation," *The International Journal of Robotics Research*, vol. 36, no. 1, pp. 86–104, 2017.
- [31] Z. Zeng, Z. Zhou, Z. Sui, and O. C. Jenkins, "Semantic robot programming for goal-directed manipulation in cluttered scenes," in *International Conference on Robotics and Automation*, 2018, pp. 7462–7469.
- [32] C. Lynch, M. Khansari, T. Xiao, V. Kumar, J. Tompson, S. Levine, and P. Sermanet, "Learning latent plans from play," *arXiv preprint arXiv:1903.01973*, 2019.
- [33] F. Codevilla, M. Müller, A. López, V. Koltun, and A. Dosovitskiy, "End-to-end driving via conditional imitation learning," in *International Conference on Robotics and Automation*, 2018, pp. 4693–4700.
- [34] A. L. Friesen and R. P. Rao, "Imitation learning with hierarchical actions," in *2010 IEEE 9th International conference on development and learning*. IEEE, 2010, pp. 263–268.
- [35] H. Dindo and G. Schillaci, "An adaptive probabilistic approach to goal-level imitation learning," in *International Conference on Intelligent Robots and Systems*, 2010, pp. 4452–4457.
- [36] A. Mandlekar, F. Ramos, B. Boots, S. Savarese, L. Fei-Fei, A. Garg, and D. Fox, "Iris: Implicit reinforcement without interaction at scale for learning control from offline robot manipulation data," in *International Conference on Robotics and Automation*, 2020, pp. 4414–4420.
- [37] D. P. Kingma and M. Welling, "Auto-encoding variational bayes," *arXiv preprint arXiv:1312.6114*, 2013.
- [38] D. G. Caldwell, S. Davis, R. J. Moreno Masey, and J. O. Gray, "Automation in food processing," in *Springer Handbook of Automation*. Springer, 2009, pp. 1041–1059.
- [39] M. Wilson, "Developments in robot applications for food manufacturing," *Industrial Robot: An International Journal*, 2010.
- [40] C. Wang, T. Luo, L. Zhao, Y. Tang, and X. Zou, "Window zooming-based localization algorithm of fruit and vegetable for harvesting robot," *IEEE Access*, vol. 7, pp. 103 639–103 649, 2019.
- [41] L. Zhang, G. Gui, A. M. Khattak, M. Wang, W. Gao, and J. Jia, "Multi-task cascaded convolutional networks based intelligent fruit detection for designing automated robot," *IEEE Access*, vol. 7, pp. 56 028–56 038, 2019.
- [42] Y. Yu, K. Zhang, L. Yang, and D. Zhang, "Fruit detection for strawberry harvesting robot in non-structural environment based on mask-rcnn," *Computers and Electronics in Agriculture*, vol. 163, p. 104846, 2019.
- [43] A. Kuznetsova, T. Maleva, and V. Soloviev, "Using yolov3 algorithm with pre-and post-processing for apple detection in fruit-harvesting robot," *Agronomy*, vol. 10, no. 7, p. 1016, 2020.
- [44] C. Huangfei et al., "Design and research on the end actuator of tomato picking robot," *Journal of Physics: Conference Series*, vol. 1314, no. 1, p. 012112, 2019.
- [45] L. Mu, G. Cui, Y. Liu, Y. Cui, L. Fu, and Y. Gejima, "Design and simulation of an integrated end-effector for picking kiwifruit by robot," *Information Processing in Agriculture*, vol. 7, no. 1, pp. 58–71, 2020.
- [46] M. Bollini, S. Tellex, T. Thompson, N. Roy, and D. Rus, "Interpreting and executing recipes with a cooking robot," in *Experimental Robotics*, 2013, pp. 481–495.
- [47] H. Zhang and S. Nikolaidis, "Robot learning and execution of collaborative manipulation plans from youtube cooking videos," *arXiv preprint arXiv:1911.10686*, 2019.
- [48] S. Davis, J. W. Casson, R. J. M. Masey, M. King, J. O. Gray, and D. G. Caldwell, "Robot prototyping in the design of food processing machinery," *Industrial Robot: An International Journal*, 2007.
- [49] S. Ma, L. Du, E. Tsuchiya, and M. Fuchimi, "made grippers for soft food grasping," in *International Conference on Ubiquitous Robots*, 2020, pp. 362–367.
- [50] H. Kim, Y. Ohmura, A. Nagakubo, and Y. Kuniyoshi, "Training robots without robots: Deep imitation learning for master-to-robot policy transfer," *arXiv preprint arXiv:2202.09574*, 2022.
- [51] D. Chotrov, Z. Uzunova, Y. Yordanov, and S. Maleshkov, "Mixed-reality spatial configuration with a zed mini stereoscopic camera," 11 2018.
- [52] A. Billard, S. Calinon, R. Dillmann, and S. Schaal, "Robot programming by demonstration," *Springer Handbook of Robotics*, pp. 1371–1394, 2008.
- [53] L. Bazzani, H. Larochelle, and L. Torresani, "Recurrent mixture density network for spatiotemporal visual attention," in *International Conference on Learning Representations*, 2016.
- [54] K. He, X. Zhang, S. Ren, and J. Sun, "Deep residual learning for image recognition," in *Conference on Computer Vision and Pattern Recognition*, 2016, pp. 770–778.
- [55] A. Vaswani, N. Shazeer, N. Parmar, J. Uszkoreit, L. Jones, A. N. Gomez, Ł. Kaiser, and I. Polosukhin, "Attention is all you need," in *Neural Information Processing Systems*, 2017, pp. 5998–6008.
- [56] J. Paillard, "Fast and slow feedback loops for the visual correction of spatial errors in a pointing task: a reappraisal," *Canadian Journal of Physiology and Pharmacology*, vol. 74, no. 4, pp. 401–417, 1996.
- [57] S. Abnar and W. Zuidema, "Quantifying attention flow in transformers," in *Annual Meeting of the Association for Computational Linguistics*, 2020, pp. 4190–4197.
- [58] Y. Kuniyoshi, M. Inaba, and H. Inoue, "Learning by Watching: Extracting reusable task knowledge from visual observation of human performance," *Transactions on Robotics and Automation*, vol. 10, no. 6, pp. 799–822, 1994.
- [59] G. Konidaris, S. Kuindersma, R. Grupen, and A. Barto, "Robot learning from demonstration by constructing skill trees," *The International Journal of Robotics Research*, vol. 31, no. 3, pp. 360–375, 2012.
- [60] C. Yu and D. H. Ballard, "Understanding human behaviors based on eye-head-hand coordination," in *International Workshop on Biologically Motivated Computer Vision*, 2002, pp. 611–619.
- [61] J. Pelz, M. Hayhoe, and R. Loeber, "The coordination of eye, head, and hand movements in a natural task," *Experimental Brain Research*, vol. 139, pp. 266–77, 2001.
- [62] M. Hayhoe and D. Ballard, "Eye movements in natural behavior," *Trends in Cognitive Sciences*, vol. 9, pp. 188–94, 2005.
- [63] H. Kim, Y. Ohmura, and Y. Kuniyoshi, "Memory-based gaze prediction in deep imitation learning for robot manipulation," *arXiv preprint arXiv:2202.04877*, 2022.
- [64] L. Liu, H. Jiang, P. He, W. Chen, X. Liu, J. Gao, and J. Han, "On the variance of the adaptive learning rate and beyond," in *International Conference on Learning Representations*, 2020, pp. 1–14.
- [65] Z. Zhong, L. Zheng, G. Kang, S. Li, and Y. Yang, "Random erasing data augmentation," in *AAAI conference on artificial intelligence*, vol. 34, no. 07, 2020, pp. 13 001–13 008.